HHS Public Access

Author manuscript

Neuron. Author manuscript; available in PMC 2021 July 08.

Published in final edited form as:

Neuron. 2020 July 08; 107(1): 144–157.e4. doi:10.1016/j.neuron.2020.04.004.

A Synaptic Circuit Required for Acquisition but Not Recall of Social Transmission of Food Preference

Cosmos Yuqi Wang[1,*], **Zhihui Liu**[1,2], **Yi Han Ng**[1], **Thomas C. Südhof**[1,2,*]

[1]Department of Molecular and Cellular Physiology, Stanford University School of Medicine, Stanford, CA 94305, USA

[2]Howard Hughes Medical Institute, Stanford University School of Medicine, Stanford, CA 94305, USA

SUMMARY

During social transmission of food preference (STFP), the combination of an olfactory sensory input with a social cue induces long-term memory of a food odor. How a social cue produces long-term learning of an olfactory input, however, remains unknown. Here, we show that the neurons of the anterior olfactory nucleus (AON) that form abundant synaptic projections onto granule cells in the olfactory bulb (OB) express the synaptogenic molecule C1ql3. Deletion of *C1ql3* in the dorsolateral AON impaired synaptic AON→OB connections and abolished acquisition but not recall of STFP memory, without significantly affecting basal olfaction. Moreover, deletion in granule cells of the OB of *Bai3*, a postsynaptic GPCR receptor for C1ql3, similarly suppressed synaptic transmission at AON→OB projections and abolished acquisition but not recall of STFP memory. Thus, synaptic AON→OB connections are selectively required for STFP memory acquisition and are formed by an essential interaction of presynaptic C1ql3 with postsynaptic Bai3.

eTOC blurb

Wang et al. show that presynaptic C1ql3 and its postsynaptic receptor Bai3, an adhesion-GPCR, are necessary for the formation of functional synaptic projections from the anterior olfactory nucleus to the olfactory bulb, and that this projection is required for the acquisition of social transmission of food preference memory in mice.

*Correspondence: C.Y.W. cosmosyw@stanford.edu; T.C.S. tcs1@stanford.edu (lead contact).

AUTHOR CONTRIBUTIONS

C.Y.W. and T.C.S. designed the experiments, C.Y.W. & Z.L. performed the experiments, C.Y.W. and T.C.S. analyzed the results, Y.H.N. supplied an unpublished essential reagent, and C.Y.W. and T.C.S. wrote the manuscripts with input from all authors.

DECLARATION OF INTERESTS

The authors declare no conflict of interest

Keywords

Learning & memory; olfactory information processing; social transmission of food preference; centrifugal projections; synapse maintenance; C1ql3; Bai3; anterior olfactory nucleus (AON); olfactory bulb (OB)

INTRODUCTION

The brain processes and transforms information at massive yet precise synaptic connections that wire trillions of neurons into millions of networks. How the brain works critically depends on the formation and function of defined synaptic connections. Synaptic connections are instructed and specified by trans-synaptic signaling molecules (Zipursky and Sanes, 2010; Südhof, 2017; Yuzaki, 2018). Many such molecules have been identified, but few instances in which a specific set of molecules instructs a defined synaptic connection were described.

C1q-like 3 (C1ql3) is a secreted neuronal protein that binds to the postsynaptic adhesion G-protein-coupled receptor (GPCR) Bai3 (gene symbol *Adgrb3*) and acts as a synaptic organizer (Bolliger et al., 2011; Kakegawa et al., 2015; Sigoillot et al., 2015; Martinelli et al., 2016; Matsuda et al., 2016; Chew et al., 2017). C1ql3 is a member of the C1ql protein family, which is part of the tumor necrosis factor (TNF)/C1Q superfamily (Kishore et al., 2004; Tom Tang et al., 2005). C1ql proteins (C1qls) are encoded by four homologous genes, C1ql1–C1ql4, that are closely related to two other members in the TNF/C1Q superfamily: cerebellins and adiponectin (Stevens et al., 2007; Matsuda et al., 2010; Uemura et al., 2010). Like these molecules, C1qls feature a globular C-terminal C1q domain that forms homotrimers. In addition, C1qls contain two smaller N-terminal domains, a cysteine-rich sequence that is homologous to a domain in cerebellins but is lacking from adiponectin, and a collagen-like sequence that is similarly found in other C1q domain proteins but is lacking from cerebellins (Yuzaki, 2018). Via these N-terminal sequences, C1qs assemble into hexamers of trimers to create a homomultimeric complex comprising 18 C1ql subunits (Ressl et al., 2015). Although the C1q domains of different proteins exhibit similar three-dimensional structures, they bind to distinct ligands. For example, the C1q domains of cerebellin-1 and -2 bind to GluD1 and GluD2 (Matsuda et al., 2010; Uemura et al., 2010), the C1q domains of C1qls bind to Bai3 (Bolliger et al., 2011; Kakegawa et al., 2015; Sigoillot et al., 2015), and the C1q domain of adiponectin binds to AdipoR1/R2 (Yamauchi et al., 2003).

C1ql3 is abundantly expressed in central olfactory regions, such as the anterior olfactory nucleus (AON) and piriform cortex (PCx) (Martinelli et al., 2016). Olfactory information enters the brain via the olfactory bulb (OB), and is relayed by mitral/tufted cells to primary olfactory cortices, AON and PCx (Nagayama, Homma and Imamura, 2014). Similar to the retina, the local circuitry of the OB processes olfactory information before relaying to the cortex. Different from the retina, however, the OB receives abundant centrifugal inputs from the central brain regions, including the AON, the PCx, and several neuromodulatory centers (Matsutani and Yamamoto, 2008). The AON→OB projections are the most abundant among these centrifugal inputs, forming synapses primarily on the granule cells in the OB (Price

and Powell, 1970; Haberly and Price, 1978; de Olmos, Hardy and Heimer, 1978; Luskin and Price, 1983; Padmanabhan et al., 2016).

In the OB, granule cells are abundant interneurons that mediate reciprocal and lateral inhibition of mitral/tufted cells via dendrodendritic synapses, and that are replenished by adult neurogenesis throughout life (Shepherd, Chen and Greer, 2004). Centrifugal synapses on granule cells indirectly modulate the physiological responses of nearly all cell types in the OB and are modified by synaptic plasticity (Halabisky and Strowbridge, 2003; Balu, Pressler and Strowbridge, 2007; Gao and Strowbridge, 2009; Boyd et al., 2012; Markopoulos et al., 2012). Moreover, the topographical organization of centrifugal synapses suggests that centrifugal projections are important behaviorally (Padmanabhan et al., 2016). However, only studies involving coarse surgical lesions of the centrifugal pathway have been performed to examine their behavioral relevance in olfactory information processing (Kiselycznyk, Zhang and Linster, 2006), and the physiological significance of AON→OB projections remains unclear.

In the present study, we used an ethologically relevant olfactory behavior – social transmission of food preference (STFP) (Galef, 2002; Wrenn, 2004) – to study how trans-synaptic organizer molecules mediate the formation/maintenance of a particular olfactory circuit, the AON→OB projection, and how this circuit contributes to the processing of olfactory sensory information. We found that C1ql3 and Bai3 are required for centrifugal AON→OB synaptic connections that in turn are essential for acquisition of STFP. Hence, we identified a molecularly and anatomically defined projection that specifically regulates the formation of STFP memory.

RESULTS

C1ql3-positive AON neurons form a hub connecting the OB to diverse brain regions.

We previously generated conditional knockin/knockout (cKO) mice that co-express mVenus with endogenous C1ql3, and allow Cre-dependent deletion of *C1ql3* and mVenus (Martinelli et al., 2016). In these mice, mVenus (and C1ql3) is abundantly produced in olfactory cortices, such as the AON and PCx. Moreover, we observed a strong mVenus signal in the granule cell layer of the OB without detectable C1q3 mRNA (Martinelli et al., 2016), suggesting that in the *C1ql3* cKO mice, mVenus is transported via axonal projections to the OB from C1ql3 positive neurons in the AON and/or PCx.

To test this hypothesis, we injected fluorescently labeled cholera toxin B (CTB), a retrograde tracer, into the OB of *C1ql3 cKO* mice, and measured the co-localization of mVenus and CTB in neurons of the AON and PCx (Figure 1A–1B). The AON is divided into two basic zones, the pars externa and pars principalis, which is further subdivided into four major divisions (pars medialis (mAON), pars lateralis (lAON), pars dorsalis (dAON) and pars ventralis (vAON)) (Brunjes, Illig and Meyer, 2005). We found that the majority (~95%) of CTB+ neurons in all subdivisions of the AON's pars principalis are positive for mVenus (Figure 1C–1D, 1I). Thus, nearly all AON→OB projecting neurons express C1ql3.

In contrast, we observed that only a minority (~25%) of PCx→OB projection neurons contain mVenus (Figure 1E–H, 1l). The PCx can be divided into anterior and posterior parts that extend in a ventral to dorsal direction analogous to the hippocampus, and are comprised of a superficial molecular layer (layer 1), a densely packed pyramidal cell layer (layer 2), and a deep polymorphic layer (layer 3) (Neville and Haberly, 2004). Although C1ql3+ neurons are abundant in the PCx, most C1ql3+ neurons were found in layer 3, whereas PCx→OB projection neurons were observed in layer 2 (Figure 1F, 1H).

To confirm and extend the retrograde tracing results, we examined the overall synaptic projections elaborated by AON neurons using SynaptoTag AAVs that co-express mCherry (which fills neural processes) and EGFP-tagged synaptobrevin-2 (which labels output synapses) (Xu and Südhof, 2013) (Figure S1). AON neurons formed abundant synaptic projections onto granule cells of the OB, confirming the CTB-tracing results (Figure 1). In addition, AON neurons projected to the PCx with decreasing density along its anterior-to-posterior axis (Figure S1D–G). Furthermore, AON neurons projected to the submedial nucleus of the thalamus, the cortical amygdala, the tegmental reticular nucleus, and the dorsal raphe nucleus where they formed synapses on serotonergic neurons (Figure S1G–I).

We next asked whether AON→PCx projection neurons also express C1ql3, and whether AON→OB and AON→PCx projection neurons overlap. Retrograde CTB tracing with two fluorescent tags revealed that much fewer AON neurons project to the PCx than to the OB (Figure S2). The majority (~65%) of the AON→PCx projection neurons also projected to the OB, whereas only a minority (~22%) of AON→OB projection neurons also projected to the PCx (Figure S2). Furthermore, retrograde activation of double-floxed SynaptoTag expressed in the AON by infection of the OB with rAAV2-retro-Cre (Tervo et al., 2016) confirmed that only a small subset of AON-neurons projecting to the OB also sends axon collaterals to the anterior PCx (Figure S3). Thus, the overall picture that emerges from these tracing studies is that the AON forms the hub of a densely interconnected network. In this network, C1ql3^{+} AON neurons act as a central node that not only link each AON to both OBs (Yan et al., 2008), but also connects the each AON to the PCx and to other brain regions.

C1ql3 expression in the AON is required for formation but not recall of STFP memory.

To probe the function of the AON and the role of C1ql3 in that function, we infected the dorsolateral AON of adult *C1ql3* cKO mice (~7–8 weeks old) with AAVs that express active Cre-recombinase (Cre) or inactive mutant Cre-recombinase (ΔCre, used as a control), both tagged with tdTomato (Figure 2A). C1ql3 was consistently deleted from ~50% of the AON in these experiments, mostly from the dorsolateral pars principalis (Figure 2B). Three to four weeks after the infection, we monitored general olfaction in the mice.Firstly, deletion of *C1ql3* in the AON had no effect on the time a mouse needed to find a buried food pellet, or on the olfactory sensitivity of mice (Figure S4A–S4B). Moreover, we gave mice the choice between cinnamon- and cocoa-scented food, and calculated food preference as the difference between consumed cinnamon-and cocoa-scented food divided by the total amount of food eaten. *C1ql3 cKO* mice preferred cocoa-scented food, and this preference was unchanged after AAV-mediated deletion of *C1ql3* in the AON (Figure 2C–2D, S4D). Thus, partial

deletion of *C1ql3* from the AON did not significantly impair basic olfactory functions or odor discrimination in mice.

We then examined whether C1ql3 expression in the AON is required for social transmission of food preference (STFP), a form of social olfactory learning (Galef, 2002; Wrenn, 2004; Bessières, Nicole and Bontempi, 2017). During STFP training, a food-restricted demonstrator mouse consumes food pellets scented with a specific cued odor, and then socially interacts for 30 min with an observer mouse in the absence of food. Subsequently, the observer mouse is given the choice between food of the cued odor or a novel odor, and the amount of each type of food consumed in a one-hour period is measured (Figure 2E–2F). In our STFP experiments, we used the innately non-preferred as the cued odor compared to the novel odor (i.e. cinnamon instead of cocoa, or acetophenone [Acp] instead of octanal [Oct]). In this manner, STFP learning involves a switch in food preference. STFP represents a one-trial learning paradigm with a memory that persists for many weeks (Bessières, Nicole and Bontempi, 2017; Liu et al., 2017).

Partial deletion of *C1ql3* in the AON prior to STFP training completely blocked STFP learning without affecting total food consumption (Figure 2E–F, S4E). *C1ql3* cKO mice with ΔCre expression in the AON showed a strong preference for cinnamon-over cocoa-scented food after STFP. In contrast, *C1ql3* cKO mice with Cre expression in the AON exhibited no such reversal in food preference (Figure 2F). The impairment of STFP persisted two weeks after training (Figure S2F), and was independent of the odor pair, as confirmed with Oct vs. Acp STFP. *C1ql3* cKO mice exhibited a strong innate preference for Oct- over Acp-scented food (Figure 2G). Partial *C1ql3* deletion in the AON also abolished STFP when Acp was used as the cued odor and Oct as the novel odor (Figure 2H, S4E). The *C1ql3* deletion in the AON had no effect on the performance of mice in the open field test or three-chamber sociability test (Figure S4G, S4H). Thus, expression of C1ql3 in the AON is essential for the acquisition a social form of memory, but does not generally alter the overall olfaction, mobility, or sociability of mice.

We next asked whether C1ql3 expression in the AON is selectively required for a specific phase of STFP memory. To address this, we deleted *C1ql3* from the AON after, instead of before, STFP training (Figure 2I). STFP testing two weeks later (a time period sufficient for mediating *C1ql3* deletion, Figure S6A–S6C) showed no effect of the *C1ql3* deletion in the AON on STFP memory (Figure 2J). Thus, full C1ql3 expression in the AON is only required for STFP learning, but not for the recall of STFP memory.

To test whether C1ql3 expression in the AON is generally required for all forms of olfactory learning, we examined a non-associative form of olfactory memory that is similar to olfactory habituation. We introduced anise and cinnamon odors into random corners of an open field, and measured the sniffing preference for these odors (‘naïve’ preference index, calculated as time investigating anise divided by that for cinnamon). 24 hours later, we exposed the same mice to the cinnamon odor for 15 min in their home cage. After a further 30 min, we re-introduced the mice to the open field containing anise and cinnamon odors (again in random corners), and measured the ‘pre-exposed’ preference index (Figure 2K). If a mouse remembered it had just sniffed the cinnamon odor, it would prefer the novel odor

anise (Rochefort et al., 2002). Thus, non-associative memory is quantified as the ratio of the pre-exposed to the naïve anise preference indices. The *C1ql3* deletion in the AON had no significant effect on this test (Figure 2L), demonstrating that C1ql3 expression in the AON is not generally required for olfactory learning. All behavior experiments were replicated with an independent cohort of mice and AAV co-expressing ΔCre/Cre and SynaptoTag (further illustrated below) (Figure S5).

C1ql3 expression in AON→aPCx projection neurons is not required for STFP memory acquisition.

Our tracing results showed that C1ql3-expressing neurons of the AON (which constitute the majority of AON neurons) project to both the OB and the PCx. Given the demonstrated importance of the PCx in olfactory memory (Choi et al., 2011; Sacco and Sacchetti, 2011; Loureiro et al., 2019), the question arises whether C1ql3 expression is required for STFP learning in AON→OB projection neurons, in AON→PCx projection neurons, or in both.

To address this question, we used a projection-specific Cre deletion strategy. We injected AAVs that co-express Cre and tdTomato in a Flp-dependent manner (fDIO-Cre-IRES-tdTomato) into the AON of *C1ql3 cKO* mice. At the same time, we injected rAAV2-retro expressing Flp into the OB or the anterior PCx. As a control, we omitted the injection of retro-Flp AAVs (Figure 3A–C). Three weeks after injections, we performed STFP experiments using cinnamon- vs. cocoa-scented food as described in Figure 2. Both the control and the anterior PCx group exhibited normal STFP learning, whereas the OB group in which AON→OB projections are targeted suffered from a complete loss of STFP learning without affecting total food consumption(Figure 3D–3F). We repeated the same experiment using Acp vs. Oct as a second odor pair, with the same results (Figure 3G–3I). Thus, the partial *C1ql3* deletion in AON→OB neurons but not in AON→aPCx projection neurons is sufficient to impair STFP memory acquisition.

C1ql3 deletion in the AON decreases AON→OB synapse numbers.

Why does deletion of *C1ql3* from AON→OB projection neurons selectively ablate STFP learning? C1ql3 could function at granule cell synapses either as a signaling molecule like adiponectin, or as a synaptogenic adaptor molecule like Cbln's (Yuzaki, 2017).

To address this question, we infected the AON of *C1ql3 cKO* mice with AAVs that co-express SynaptoTag (using a tdTomato-version of SynaptoTag to visualize presynaptic terminals in red) and mutant inactive ΔCre or wild-type active Cre (Figure 4A–4B). Four weeks afterwards, we quantified the number of AON→OB synapses in the granule cell layer of the OB via their SynaptoTag signals (Figure 4C–4D). Compared to the ΔCre control, Cre deletion of *C1ql3* in the AON greatly reduced (~65%) the density of AON→OB synapses in less than 2 weeks (Figure 4E; S6A–S6C). The synapse loss was not due to viral toxicity because injection of the same batch of ΔCre vs. Cre viruses into the AON of wild-type C57BL/6J mice had no significant effect on synapse numbers (Figure S6D–S6F), and the AON *C1ql3* deletion did not affect neuronal survival (Figure S6K). Note that the viruses used in these experiments were validated in STFP experiments (Figure S5), confirming the relevance of the morphological results.

To extend our SynaptoTag results, we analyzed the density of different synaptic markers in the local OB circuitry as a function of AON *C1ql3* deletion, using vGluT1 as a marker of excitatory synapses and synaptophysin-2 (a.k.a. synaptoporin) as a marker of inhibitory dendrodendritic synapses (Fykse et al., 1993; Whitman and Greer, 2007; Kelsch, Sim and Lois, 2010) (Figure 4F, 4G). The granule cell layer (GCL) and the external plexiform layer (EPL) both contained a high density of excitatory synapses, while inhibitory dendrodendritic synapses were detected mostly in the EPL (Figure 4G). The AON *C1ql3* deletion caused a modest decrease in excitatory synapse density particularly in the GCL, without a change in inhibitory synapses (Figure 4H). Thus, the partial *C1ql3* deletion in the AON decreases AON→OB synapse numbers without disrupting the majority of synaptic connections in the OB.

Finally, we asked whether the *C1ql3* deletion also affects AON→PCx synapse numbers. Using the same SynaptoTag approach (Figure 4I–4J), we found that the AON *C1ql3* deletion induced a significant reduction (~35%) in AON→PCx synapses in the rostral anterior PCx, caused a trend towards a synapse reduction (~20%) in the caudal anterior PCx, and had no effect in the posterior PCx (Figure 4K). Since C1ql3 is primarily expressed in AON neurons projecting to the anterior PCx (see Figure S2, S3), these results suggest that C1ql3 is also essential for synapses formed by these neurons (most of which also project to the OB), but is not essential for other AON→PCx projection neurons.

Deletion of *C1ql3* in the AON severely impairs synaptic transmission at AON→OB granule cells synapses.

To investigate whether the AON *C1ql3* deletion alters the function of AON→OB granule cell synapses, we recorded synaptic responses from granule cells in acute OB slices (Figure 5A). Deletion of *C1ql3* in the AON had no effect on the capacitance of granule cells, but caused a large decrease (~65%) in the frequency and a smaller (~20%) but significant decrease in the amplitude of spontaneous EPSCs (sEPSCs) (Figure 5B–5F). No change in sEPSC kinetics was observed. Recordings of evoked EPSCs by stimulation of centrifugal fibers (monitored via input/output curves in order to control for differences in electrode placements and stimulus strength) revealed that the *C1ql3* deletion in the AON greatly impaired synaptic transmission to granule cells, again without a change in kinetics (Figure 5G–5I). Both the coefficient of variation and paired-pulse ratios were significantly increased after *C1ql3* deletion in the AON, suggesting that the loss of AON→OB synaptic transmission was due, at least in part, to a decrease in release probability (Figure 5J, 5K). Viewed together, these findings indicate that the *C1ql3* deletion in the AON causes a nearly complete block in the function (Figure 5) of AON→OB granule cell synapses, suggesting that the *C1ql3* deletion not only decreases synapse numbers (Figure 4) but also impairs synapses functionally. Note that although the electrical stimulation does not specifically activate AON→OB axonal projections, the fact that most centrifugal projections to OB granule cells originate from the AON (Padmanabhan et al., 2019) and that our manipulation is presynaptic at the AON indicate that the observed deficit indeed reflects a loss of AON→OB synaptic transmission.

Bai3 serves as a postsynaptic C1ql3 receptor at AON→OB granule cell synapses that is essential for STFP learning.

Bai3 is an adhesion GPCR (gene symbol *Adgrb3*) that binds C1ql's with high affinity (Bolliger et al., 2011; Kakegawa et al., 2015). To test the possibility that Bai3 in OB granule cells serves as a receptor for C1ql3 at AON→OB synapses, we infected the granule cell layer of the OB of Bai3 *cKO* mice (Kakegawa et al., 2015) with AAVs expressing EGFP-tagged ΔCre (as a control) or Cre (Figure 6A). At the same time, we infected the AON with SynaptoTag viruses (Figure 6A). Quantitative RT-PCR revealed that Cre-expression reduced Bai3 mRNA expression in the GCL (Figure 6B). The partial reduction in mRNA levels could be due to incomplete infection of the GCL with Cre (Figure 6C). Analysis of the density of SynaptoTag puncta in the granule cell layer of the OB showed that the Bai3 deletion significantly but modestly (~30%) reduced the density of AON→OB granule cell synapses without altering neuronal survival (Figure 6D–6E, S6L). In these experiments, the SynaptoTag density was compared in ΔCre- vs. Cre-infected OBs from the same mouse and in Cre+ vs. Cre- sections of the same OB, enabling an accurate assessment of the effect of the Bai3 deletion.

These results are consistent with the notion that presynaptic C1ql3 acts by binding to postsynaptic Bai3, but C1ql3 also acts as a trans-synaptic adaptor binding to presynaptic neurexin-3 (Nrxn3) and to postsynaptic kainate receptors (Matsuda et al., 2016). To test whether C1ql3-binding to Nrxn3 may account, at least in part, for the phenotype, we deleted *Nrxn3* in the AON using *Nrxn3* cKO mice (Aoto et al., 2015). However, using SynaptoTag labeling revealed no effect of the *Nrxn3* deletion on the density of AON→OB synapses, ruling out this pathway (Figure S6G–S6J).

We next examined the effect of the *Bai3* deletion in OB granule cells on synaptic transmission. Recordings of evoked EPSCs by centrifugal fiber stimulation in acute OB slices showed that the Bai3 deletion almost completely ablated synaptic transmission, and additionally increased the EPSC rise times of the remaining EPSCs (Figure 7B–7D). Moreover, the *Bai3* deletion increased the coefficient of variation of EPSCs, and the paired-pulse ratio without changing the cell capacitance (Figure 7A, 7E–7F), suggesting a major decrease in release probability. Overall, these data show that similar to the *C1ql3* deletion in the AON, the *Bai3* deletion in the OB causes an almost complete loss of synapse function that is due, at least in part, to a decrease in release probability, with the modest decrease in synapse density induced by the Bai3 deletion (Figure 6) likely a secondary consequence of the synapse dysfunction (Figure 7).

The fact that the *Bai3* deletion is postsynaptic raises the question whether Bai3 is selectively required for centrifugal synaptic inputs that are largely derived from the AON (Padmanabhan et a., 2019), or for all synaptic inputs on granule cells. To address this question, we examined dendrodendritic synaptic inputs from mitral/tufted cells onto granule cells. We selectively stimulated these inputs with an electrode placed in the external plexiform layer (Figure S7A). Strikingly, the postsynaptic Bai3 deletion in granule cells greatly increased mitral/tufted cell→granule cell synaptic transmission, as revealed by input/output curves of the peak EPSC amplitude (>100% increase) and charge transfer (~300% increase) (Figure S7B–S7D). No change in the evoked EPSC kinetics, coefficient of

variation, or paired-pulse ratio was detected (Figure S7E–S7G). The larger increase in charge transfer compared to peak amplitude could be explained by lateral excitation of mitral/tufted cells which causes prolonged network activation (Christie & Westbrook, 2006). Moreover, the increase in dendrodendritic excitation could explain the increase in eEPSC rise times observed in Fig. 7D, because proximal stimulation could antidromically activate mitral/tufted cells to a limited extent. Direct measurements of the amplitude ratios of EPSCs elicited by stimulation of centrifugal afferent fibers (proximal stimulation) vs. mitral/tufted cell inputs (distal stimulation) showed that the *Bai3* deletion decreased this ratio by ~90% (Figure S7H). Since the OB lacks C1ql3 expression (Martinelli et al., 2016), these data together with those described above suggest that Bai3 maintains the synaptic strength of centrifugal projections by interacting with C1ql3 from AON→OB projection neurons, but simultaneously suppresses dendrodendritic excitatory inputs from mitral/tufted cells via unknown mechanisms.

Above we hypothesized that the *C1ql3* deletion in the AON blocks STFP learning because it impairs synaptic transmission at AON→OB synapses. If this hypothesis was correct, the *Bai3* deletion in the OB should have the same behavioral phenotype, except if the increased dendrodendritic excitation compensated for the loss of centrifugal inputs. To address this question, we measured STFP in mice as a function of the *Bai3* deletion in OB granule cells (Figure 8A). In these experiments, we consistently deleted *Bai3* from ~70% of the GCL of the OB (Figure 8B). The postsynaptic *Bai3* deletion had no effect on innate food preference (Figure 8C, 8D), but blocked STFP learning when instituted before STFP training (Figure 8E, 8F). In contrast but similar to the deletion of *C1ql3*, the *Bai3* deletion did not impair STFP memory after STFP training (Figure 8G, 8H). The effect of the *Bai3* deletion was selective for STFP odor learning, as it did not alter total food consumption during the various tests, increase the time it took a mouse to find a buried food pellet, or decrease olfactory sensitivity (Figure S8A–S8C). Moreover, the *Bai3* deletion in the OB did not alter the behavior of mice in open field tests or the three-chamber sociability test (Figure S8C–S8D). Finally, the *Bai3* deletion in the OB did not affect non-associative olfactory learning (Figure 8I–8J). Thus, the *Bai3* deletion in the OB causes the same behavioral phenotype as the *C1ql3* deletion in the AON, consistent with the notion that STFP learning, but not STFP memory recall or other olfactory behaviors examined, require intact C1ql3-mediated Bai3 signaling at AON→OB synapses.

DISCUSSION

In the present study, we employed genetic manipulations of an interacting pair of trans-synaptic organizer molecules – C1ql3 and Bai3 – to probe the function of the AON→OB circuit in STFP memory. Our results enable three major conclusions that provide a new perspective on the role of centrifugal projections from the AON to the OB.

First, most C1ql3-positive AON neurons form synaptic projections on granule cells in the OB, whereas a minority establishes synapses on pyramidal neurons in the anterior PCx and on neurons in additional brain regions, such as the cortical amygdala and the raphe (Figure 1, S1–S3). Thus, the C1ql3 positive neurons in the AON act as a hub connecting peripheral OB and multiple central brain regions.

Second, expression of C1ql3 in AON→OB projection neurons and of Bai3 in OB granule cells is essential for the function of AON→OB granule cell synapses. Deletion of either *C1ql3* in the AON or of *Bai3* in the OB causes a partial loss of these synapses and a nearly complete ablation of their function. Since the genetic deletions have much bigger effects on the function than on the number of AON→OB synapses, it is likely that synapse loss is secondary to the severe impairment in synaptic transmission. This impairment involves, at least in part, a decrease in release probability. Thus, the binding of presynaptic C1ql3 to postsynaptic Bai3 receptors is likely an essential component of the machinery that renders AON→OB granule cell synapses functional. The increased synaptic strength of dendrodendritic excitatory inputs from mitral/tufted cells onto *Bai3*-deleted granule cells suggests that *Bai3*-mediated centrifugal synapses selectively required C1ql3 as its presynaptic partner.

Third and possibly most importantly, synaptic transmission at synapses from by dorsolateral AON neurons on OB granule cells is essential for STFP learning, but not for basal olfaction, non-associative olfactory memory, or even STFP memory storage and recall. This selective requirement was demonstrated using as a tool the deletion of either *C1ql3* in the AON (Figure 2, S4) or of *Bai3* in the OB (Figure 8, S8). Our results thus indicate that the abundant AON→OB granule cell projection performs a crucial function in long-term memory acquisition. The phenotype described here differs remarkably from our earlier observation that IGF1-dependent LTP in mitral cell/granule cell dendrodendritic inhibition is also involved in STFP memory (Liu et al., 2017). Specifically, we found earlier that IGF1-dependent LTP is required for the stable maintenance of STFP memory (Liu et al., 2017). Blocking this type of LTP by deletion of synaptotagmin-10 or of IGF1 receptors only had a modest effect on STFP memory immediately after training, but more prominently several weeks after training (Liu et al., 2017). The present study, in contrast, shows that suppression of AON→granule cell synaptic transmission blocks STFP memory acquisition. Thus, this synaptic connection does not act by enabling dendrodendritic synapse LTP, but encodes a key signal that instructs the olfactory memory of the OB.

Viewed together, our three conclusions define the molecular basis for a synaptic connection that is selectively essential for establishing but not maintaining or recalling a social form of olfactory memory. As always with an unexpected observation, our findings raise new questions. First, how does the binding of C1ql3 to Bai3 render synapses functionally competent? Clearly high-affinity binding of C1ql3 to Bai3 (and probably other Bai isoforms) is important for synapses, but its mechanism of action remains to be explored. Our data demonstrate that when either *C1ql3* or *Bai3* are deleted in a fully developed brain, synapse numbers are decreased modestly but synaptic transmission is severely impaired, suggesting that C1ql3 binding to Bai3 is required primarily for maintaining the functionality of synapses, and secondarily for maintaining their structural integrity. A major question now is whether C1ql3 operates as a hormone-like molecule analogous to adiponectin to which it is highly homologous, or like an adaptor protein analogous to Cbln's that links an unknown presynaptic adhesion molecule to postsynaptic Bai3 (Yuzaki, 2018). One possibility was that Nrxn3 is a presynaptic receptor for C1ql3 (Matsuda et al., 2016), but our data argue against this idea (Figure S6H–S6J).

Another major question is how the AON→OB granule cell synapse enables STFP learning. Clearly this synapse does not act by gating dendrodritic LTP because the loss of that LTP has a much more modest behavioral phenotype and only destabilizes STFP memory (Liu et al., 2017), whereas the suppression of AON→OB granule cell synaptic transmission blocks STFP learning. Despite much work on local circuitry of OB, the function of granule cells is incompletely understood. Our results support the notion that the modulation on mitral/tufted cells by granule cells is highly regulated by centrifugal inputs and is essential for olfactory information processing during sophisticated behaviors like STFP.

One possibility is that the AON→OB projections are required for increasing the likelihood of granule cell spiking for lateral inhibition. In many neural circuits, lateral inhibition is crucial for successful learning and pattern separation (Cayco-Gajic & Silver, 2019). In the olfactory bulb, dendrodendritic synapses between mitral/tufted cells and granule cells mediate reciprocal and lateral inhibition. However, paired recordings between mitral cell and granule cell showed that the dendrodendritic excitation onto granule cells is weak (Pressler and Strowbridge, 2017), and *in vivo* recordings demonstrated that granule cells fire sparse action potentials (Cazakoff et al., 2014). Hence, the weak excitation of granule cells by mitral/tufted cells alone likely induces only rarely lateral inhibition. In order to achieve lateral inhibition, granule cells need to generate action potentials and transform the excitatory input from a mitral/tufted cell in one dendritic branch into an inhibitory output in another branch. Computational modeling revealed that cortical centrifugal excitation onto granule cells can produce a disproportionate enhancement of granule cell firing, thereby facilitating lateral inhibition (Pressler and Strowbridge, 2017). A likely model thus is that lateral inhibition facilitated by AON→OB synapses is required for STFP acquisition by increasing the contrast of cued odor signals during learning. Moreover, if the model is correct, such increased excitability from centrifugal inputs could not be simply compensated by an increase in dendrodendritic inputs, because after *Bai3* deletion in OB the increase in dendrodendritic excitation could not compensate for the loss of centrifugal inputs during STFP acquisition.

At a systems level, the transformation of olfactory and social information during acquisition, storage, and recall of STFP memory occurs at multiple circuit levels, with the AON serving as a central node in these processes. In the OB, IGF1 signaling is required for the maintenance of STFP memory by mediating glomerulus-specific long-term potentiation of dendrodendritic inhibition (Liu et al., 2017). In central brain regions, conversely, the hippocampus is required for the acquisition as well as for the retrieval of recent STFP memory (Clark et al., 2002; Lesburguères et al., 2011). Neurons in the orbitofrontal cortex are tagged during the early phase of STFP training and consolidation, and are activated and required for remote STFP memory retrieval (Ross and Eichenbaum, 2006; Lesburguères et al., 2011). Moreover, recent work showed that a synaptic pathway from PCx to the medial prefrontal cortex and then to the N. accumbens contribute to the recall of STFP memory (Loureiro et al., 2019). Our experiments add a further piece to this puzzle by demonstrating that in addition to these previously described circuits, the AON→OB projection is specifically required for STFP memory acquisition, supporting the notion that memory acquisition involves the parallel operation of multiple circuits at different levels of sensory information processing.

STAR★METHODS

RESOURCE AVAILABILITY

Lead Contact—Further information and requests for resources and reagents should be directed to and will be fulfilled by the Lead Contact, Thomas C. Südhof (tcs1@stanford.edu).

Materials Availability—Plasmids generated in this study for virus production are available upon reasonable requests.

Data and Code Availability—No code is generated in this study. Datasets are available upon reasonable requests.

EXPERIMENTAL MODEL AND SUBJECT DETAILS

C1ql3 cKO mice have been described previously and were maintained on a hybrid background (Martinelli et al., 2016). *Bai3 cKO* mice were generous gift from Michisuke Yuzaki (Kakegawa et al., 2015) and were maintained on a *C57BL/6J* background. *C57BL/6J* mice were purchased from the Jackson Laboratory and used for tracing experiments. Mice were group-housed (maximum of five mice per cage) and maintained on a 12 h light–dark cycle (7 am to 7 pm, light), with access to food and water *ad libitum*. Male adult mice (7–8 weeks old at time of viral injection) were used for brain morphology, tracing and behavioral experiments. Juvenile male mice (3–4 weeks old at time of viral injection) were used for electrophysiological recordings. All experiments involving animals were approved by the Stanford Animal Use Committees (IACUC and APLAC).

METHOD DETAILS

AAV preparation.—The adeno-associated virus (AAV) serotype used in this study was AAV-DJ, as well as rAAV2-retro for retrograde tracing experiments (Tervo et al., 2016). HEK293T cells were transfected, using calcium phosphate, with the AAV vector, along with the helper and serotype-specific capsid plasmids. Cells were harvested 72 h post-transfection. Nuclei were lysed and underwent iodixanol gradient ultracentrifugation (3 h at 65,000 rpm using a S80AT3 rotor). AAV were then concentrated and dialyzed in minimal essential media (MEM).

Stereotactic injections.—Mice were prepared for stereotactic injections using standard procedures approved by the Stanford University Administrative Panel on Laboratory Animal Care. For anesthesia, the stock solution was made of dissolving 5 g tribromoethanol into 5 mL T-amyl alcohol, and further diluted 80 folds into PBS to make the working solution. 0.2 mL working solution per 10 grams body weight of mouse was used for anesthesia before mounting the mouse in the stereotax. The coordinates (AP/ML/DV from Bregma) and volumes for the intercranial injections are as follows: (1) AON: +3.1/±1.25/−2.6 with 0.5 uL virus, (2) OB: +4.3/±0.85/−1.7 and +5.3/±0.6/−1.5 with 0.75 uL virus or CTB in each site, and (3) rostral aPCx: +2.0/±2.7/−3.25 with 0.75 uL virus or CTB. The CTB (Figures 1 and S2) and SynaptoTag virus (Figure S1 and S3) injections were unilateral, while all other injections were performed bilaterally.

Behavioral experiments.—All behaviors were assessed in adult male mice 3–4 weeks after viral injections.

Open field test.: Mice were individually placed in a 40 × 40 × 40 cm^3 white plastic chamber in a well-lit room and allowed to move freely for 10 min. Locomotor and exploratory behaviors were recorded using a Viewer III tracking system (Biobserve). Total distance traveled and time spent in the 20 × 20 cm^2 center of the square were quantified.

Three-chamber sociability test.: A transparent three-chamber apparatus (60 × 30 × 30 cm^3 per chamber) was used for sociability tests. For habituation, the subject was placed in the center chamber and allowed to explore the entire apparatus for 5 min, during which they were recorded using the Viewer III tracking system. The peripheral chamber (left or right) in which the mouse spent more time was designated the preferred side. Subsequently, a stranger C57BL/6J mouse was placed underneath an upside-down black wire-mesh cup within the non-preferred chamber. A novel Lego toy was placed under the same type of cup within the preferred chamber. The subject was allowed to explore the box for 10 min, during which they were recorded using the Viewer III tracking system. Time spent in each chamber was quantified, and the sociability index was calculated by dividing the time spent in the stranger mouse-containing chamber by the time spent in the Lego-containing chamber.

Buried food-finding test.: After 24 h of food deprivation, the subject was placed in a new cage containing 3 cm of bedding and a 5 g food pellet buried in a random corner of the cage. The time it took for the mouse to dig up the food pellet was recorded.

Olfactory sensitivity test.: Cinnamon extract was diluted in distilled water in 1:100, 1:1000 and 1:10000 series. 100 μL of the odor was applied onto a filter paper and attached to a random corner in the open field. The mouse was allowed to freely explore the field and recorded. The time the mouse spent investigating each odor dilution was quantified.

Non-associative olfactory memory.: This behavioral paradigm was adapted from Rochefort et al. (2002). The odors were generated by making a 1% cinnamon extract or anise extract suspension in distilled water. Next, 100 μL of the 1% cinnamon or 1% anise solution was applied to filter paper. During the initial preference test, the subject was placed in the same chamber used in the open field test, but with 1% cinnamon- and 1% anise-containing filter paper placed randomly in two separate corners. The time spent sniffing the odors within a 10 min period was recorded using the Viewer III tracking system. The anise preference index was calculated by dividing the time spent investigating anise by the time spent investigating cinnamon. 24 h later, the subject was exposed to the cinnamon odor in its home cage for 15 min. After a 30 min interval, the subject was re-introduced the open field chamber containing the anise and cinnamon odors in random corners. Time spent sniffing each odor was monitored for 10 min. The non-associative memory index was calculated by dividing the anise preference index on the second day (pre-exposed case) by that of the first day (naïve case).

Scented food production.: Normal food pellets, to which mice had access when allowed to feed *ad libitum*, were blended into powders. 100 g powdered food was mixed with: (1) 1 g of

cinnamon powder, (2) 2 g of cocoa powder, (3) 1 mL of octanal solution, or (4) 1 mL of acetophenone solution. 50 mL of deionized water was added to the mixture. The mixture was molded into cookie shape (~ 2 g per piece) and left to air dry overnight.

Innate food preference.: After 24 h of food restriction, subjects were given two food choices (1% cinnamon and 1% cocoa, or 1% octanal and 1% acetophenone) and allowed to consume them freely for 1 h. The food was weighed before and after consumption.

Social transmission of food preference (STFP).: STFP can be separated into a training and a test phase. Prior to STFP training, demonstrator and observer mice (subject; virus injected) were single-housed and food restricted for 24 h. The demonstrator mouse was placed in a new cage, given scented food (1% cinnamon or 1% acetophenone), and allowed to consume it freely for 30 min. The demonstrator mouse was moved into the cage housing the observer mouse, and they were allowed to interact freely for 30 min. During the STFP test, the observer mouse was given two food choices ([1% cinnamon and 1% cocoa] or [1% octanal and 1% acetophone]) and allowed to consume them freely for 1 h. The weight of the food was recorded before and after consumption.

Immunohistochemistry.—Mice were anesthetized by isoflurane inhalation and transcardially perfused with 20 mL PBS, followed by 25 mL 4% paraformaldehyde (PFA) diluted in PBS. Brains were extracted and post-fixed in 4% PFA for either 1 h (for synaptic marker staining) or overnight at 4°C for GFP staining and no staining. After post-fixation, brains were washed three times with PBS and cryoprotected in 30% sucrose in PBS for 24–36 h. Brains were sectioned coronally at 40 μm using a cryostat. For CTB and SynaptoTag tracing experiments, slices were mounted directly onto a positively-charged glass slides and imaged directly. Otherwise, floating slices were collected in PBS. For immunostaining, the slices were blocked and permeabilized in 5% normal goat serum and 0.3% Triton X-100-containing PBS for 1 h at room temperature. Primary antibodies against GFP (Invitrogen, 1:1000), vGluT1 (Millipore, 1:1000), synaptophysin-2 (Fykse et al., 1993, code Y941, 1:1000) or NeuN (Millipore, 1:1000) were diluted in blocking buffer and brain slices were incubated with primary antibody overnight at 4°C. After three 10 min washes in PBS, slices were incubated with secondary antibodies: Alexa Fluor-488, −555 or −647. Slices underwent three 10 min washes in PBS and were mounted on positively-charged glass slides, allowed to dry, and coverslipped.

Image acquisition and analysis.—A Nikon A1RSi confocal microscope was used to acquire all images. Images are analyzed using Nikon analysis software. Within each set of experiments, the laser power, gain, offset, and pinhole size for each laser were kept constant. For cell counting in CTB tracing experiments, cells were counted manually, with at least 5 sections analyzed per brain. For quantification of synaptic puncta, z-stack images were obtained by at 0.5 μm intervals and three slices (1 μm thickness in total) with highest signal were maximally projected. Automated background subtraction was performed using a rolling ball algorithm with a 1 μm radius. The same threshold was applied to each set of experiments and puncta parameters were automatically obtained using the analysis software. For quantification in the olfactory bulb, the entire olfactory bulb was sliced. Five sections

with 400 μm anterior-posterior distance spacing were quantified, and each data point is an average of all slices quantified. The images were taken at either medial or lateral olfactory bulb and were chosen randomly. For quantification of puncta in the PCx, three images from each subpart of PCx was used. Only the ventral PCx was imaged, and ROI was selected between layer 1 and layer 2 with equal area from each layer. For quantification of the extent of *C1ql3* deletion, three slices evenly spaced across anterior-posterior axis of AON were quantified, and the fraction of mVenus negative region over the entire AON was calculated and averaged over all three slices. For gcl coverage in OB, three slices evenly spaced across anterior-posterial axis of OB were quantified, and the fraction of Cre positive gcl region over the entire gcl was calculated and averaged over all three slices. All IHC data were collected and analyzed blindly.

Quantitative real-time PCR.—For quantification of Bai3 mRNA, virally-injected Bai3 cKO mice were anesthetized by isoflurane inhalation and decapitated, and their brains were extracted. Brains were dissected in cold PBS and 1 mm-thick coronal olfactory bulb slices were obtained using a vibratome. Granule cells and the outer part of olfactory bulb were identified under a dissection microscope and manually dissected for RNA extraction. Quantitative RT-PCR was performed in triplicates for each condition. 20 ng RNA was used each reaction, in conjunction with VeriQuest master-mix (Affymetrix) and gene-specific qRT-PCR probes (IDT).

Electrophysiology.—Three weeks after viral injection, mice were anesthetized via isoflurane inhalation and brains were quickly removed. The brain was sliced in ice-cold oxygenated (95% O_2 and 5% CO_2) cutting solution (228 mM sucrose, 11 mM glucose, 26 mM $NaHCO_3$, 1 mM NaH_2PO_4, 2.5 mM KCl, 7 mM $MgSO_4$, and 0.5 mM $CaCl_2$). Horizontal sections (300 μm thickness) were obtained using a vibratome and placed in oxygenated artificial cerebrospinal fluid (ACSF; 119 mM NaCl, 2.5 mM KCl, 1 mM NaH_2PO_4, 1.3 mM $MgSO_4$, 26 mM $NaHCO_3$, 10 mM glucose, and 2.5 mM $CaCl_2$) at 32°C for 30 min. Slices were allowed to recover at room temperature for an additional 30 min. The recording chamber was temperature controlled and set to 32°C, and ACSF was perfused at 1 mL/min. The internal solution for whole-cell patch clamp contained 135 mM CsCl, 10 mM HEPES, 1 mM EGTA, 1 mM Na-GTP, 4 mM Mg-ATP and 10mM QX314-bromide, pHed to 7.25. Only mature granule cells within the olfactory bulb were used for recordings. They were identified as having fast-kinetic sodium currents immediately after break-in when the voltage clamp was ramped from −70 to 0 mV. The fast-kinetic currents could be abolished 2 min after break-in due to the presence of QX-314 in the patch pipet. Spontaneous EPSCs (sEPSCs) were recorded at −70 mV. Evoked EPSCs (eEPSCs) were recorded at −70 mV with a concentric bipolar electrode placed within a constant distance near the mature granule cell being recorded from, 30 μm below the surface of the slice. All recordings were analyzed in Clampfit after applying a 400 Hz Gaussian filter. Rise time was defined as the time from 10% to 90% of peak amplitude, and decay time was defined as the time from 90% to 10% of peak amplitude. The experimenter was blind to the treatment groups during recordings and analysis.

QUANTIFICATION AND STATISTICAL ANALYSIS

All experiments of behavioral tests, morphological analysis and slice physiology were performed and analyzed blindly to the experimental condition. Statistics is done with Prism 8, GraphPad. Student's t test was used whenever the comparison is between two groups. The Kolmogorov-Smirnov test was used to analyze the cumulative curves. Oneway ANOVA with Bonferroni's multiple hypothesis correction was used for comparison among more than two groups. Two-way ANOVA was used for comparison of multiple groups with multiple factors. The statistical test used for each experiment was specified in the figure legend. The "*n*" used for these analyses represents number of mice (Figures 2, 3, 4, 6, 8, S4, S5, S6, S8) or number of cells (Figures 5, 7, S7), all of which have been specified in Figure Legends.

Supplementary Material

Refer to Web version on PubMed Central for supplementary material.

ACKNOWLEDGEMENTS

We thank Dr. Michisuke Yuzaki (Keio University) for providing *Bai3 cKO* mice. This work was supported by a Stanford Graduate Fellowship (to C.Y.W.), Stanford Interdisciplinary Graduate Fellowship (to C.Y.W.) and a grant from NIMH (MH052804 to T.C.S.).

REFERENCES

Aoto J, Földy C, Ilcus SMC, Tabuchi K, and Südhof TC (2015). Distinct circuit-dependent functions of presynaptic neurexin-3 at GABAergic and glutamatergic synapses. Nat. Neurosci 18, 997–1007. [PubMed: 26030848]

Balu R, Pressler RT, and Strowbridge BW (2007). Multiple modes of synaptic excitation of olfactory bulb granule cells. J. Neurosci 27, 5621–5632. [PubMed: 17522307]

Bessières B, Nicole O, and Bontempi B (2017). Assessing recent and remote associative olfactory memory in rats using the social transmission of food preference paradigm. Nat. Protoc 12, 1415–1436. [PubMed: 28686584]

Bolliger MF, Martinelli DC, and Südhof TC (2011). The cell-adhesion G protein-coupled receptor BAI3 is a high-affinity receptor for C1q-like proteins. Proc. Natl. Acad. Sci. USA 108, 2534–2539. [PubMed: 21262840]

Boyd AM, Sturgill JF, Poo C, and Isaacson JS (2012). Cortical Feedback Control of Olfactory Bulb Circuits. Neuron 76, 1161–1174. [PubMed: 23259951]

Brunjes PC, Illig KR, and Meyer EA (2005). A field guide to the anterior olfactory nucleus (cortex). Brain Res. Rev 50, 305–335. [PubMed: 16229895]

Cayco-Gajic NA, and Silver RA (2019). Re-evaluating Circuit Mechanisms Underlying Pattern Separation. Neuron 101, 584–602. [PubMed: 30790539]

Cazakoff BN, Lau BYB, Crump KL, Demmer HS, and Shea SD (2014). Broadly tuned and respiration-independent inhibition in the olfactory bulb of awake mice. Nat. Neurosci 17, 569–576. [PubMed: 24584050]

Chew KS, Fernandez DC, Hattar S, Südhof TC, and Martinelli DC (2017). Anatomical and Behavioral Investigation of C1ql3 in the Mouse Suprachiasmatic Nucleus. J. Biol. Rhythms 32, 222–236. [PubMed: 28553739]

Choi GB, Stettler DD, Kallman BR, Bhaskar ST, Fleischmann A, and Axel R (2011). Driving opposing behaviors with ensembles of piriform neurons. Cell 146, 1004–1015. [PubMed: 21925321]

Christie JM, and Westbrook GL (2006). Lateral excitation within the olfactory bulb. J. Neurosci 26, 2269–2277. [PubMed: 16495454]

Clark RE, Broadbent NJ, Zola SM, and Squire LR (2002). Anterograde amnesia and temporally graded retrograde amnesia for a nonspatial memory task after lesions of hippocampus and subiculum. J. Neurosci 22, 4663–4669. [PubMed: 12040072]

de Olmos J, Hardy H, and Heimer L (1978). The afferent connections of the main and the accessory olfactory bulb formations in the rat: an experimental HRP-study. J. Comp. Neurol 181, 213–244. [PubMed: 690266]

Fykse EM, Takei K, Walch-Solimena C, Geppert M, Jahn R, De Camilli P, and Südhof TC (1993) Relative properties and localizations of synaptic vesicle protein isoforms: The case of the synaptophysins. J. Neurosci 13, 4997–5007. [PubMed: 8229211]

Galef BG (2002). Social learning of food preferences in rodents : Rapid Appetitive Learning. In Current Protocols in Neuroscience, pp. 8.5D.1–8.5D.8. [PubMed: 18428573]

Gao Y, and Strowbridge BW (2009). Long-term plasticity of excitatory inputs to granule cells in the rat olfactory bulb. Nat. Neurosci 12, 731–733. [PubMed: 19412165]

Haberly LB, and Price JL (1978). Association and commissural fiber systems of the olfactory cortex of the rat. II. Systems originating in the olfactory peduncle. J. Comp. Neurol 181, 781–807. [PubMed: 690285]

Halabisky B, and Strowbridge BW (2003). Gamma-frequency excitatory input to granule cells facilitates dendrodendritic inhibition in the rat olfactory Bulb. J. Neurophysiol 90, 644–654. [PubMed: 12711716]

Kakegawa W, Mitakidis N, Miura E, Abe M, Matsuda K, Takeo YH, Kohda K, Motohashi J, Takahashi A, Nagao S, et al. (2015). Anterograde C1ql1 signaling is required in order to determine and maintain a single-winner climbing fiber in the mouse cerebellum. Neuron 85, 316–329. [PubMed: 25611509]

Kelsch W, Sim S, and Lois C (2010). Watching synaptogenesis in the adult brain. Annu. Rev. Neurosci 33, 131–149. [PubMed: 20572770]

Kiselycznyk CL, Zhang S, and Linster C (2006). Role of centrifugal projections to the olfactory bulb in olfactory processing. Learn. Mem 13, 575–579. [PubMed: 16980549]

Kishore U, Gaboriaud C, Waters P, Shrive AK, Greenhough TJ, Reid KBM, Sim RB, and Arlaud GJ (2004). C1q and tumor necrosis factor superfamily : modularity and versatility. Trends Immunol. 25, 551–561. [PubMed: 15364058]

Lesburguères E, Gobbo OL, Alaux-Cantin S, Hambucken A, Trifilieff P, and Bontempi B (2011). Early Tagging of Cortical Networks Is Required for the Formation of Enduring Associative Memory. Science 331, 924–927. [PubMed: 21330548]

Liu Z, Chen Z, Shang C, Yan F, Shi Y, Zhang J, Qu B, Han H, Wang Y, Li D, et al. (2017). IGF1-Dependent Synaptic Plasticity of Mitral Cells in Olfactory Memory during Social Learning. Neuron 95, 106–122. [PubMed: 28683263]

Loureiro M, Achargui R, Flakowski J, Zessen R. Van, Stefanelli T, Pascoli V, and Lüscher C (2019). Social transmission of food safety depends on synaptic plasticity in the prefrontal cortex. Science 364, 991–995. [PubMed: 31171697]

Luskin MB, and Price JL (1983). The topographic organization of associational fibers of the olfactory system in the rat, including centrifugal fibers to the olfactory bulb. J. Comp. Neurol 216, 264–291. [PubMed: 6306065]

Markopoulos F, Rokni D, Gire DH, and Murthy VN (2012). Functional properties of cortical feedback projections to the olfactory bulb. Neuron 76, 1175–1188. [PubMed: 23259952]

Martinelli DC, Chew KS, Rohlmann A, Lum MY, Ressl S, Hattar S, Brunger AT, Missler M, and Südhof TC (2016). Expression of C1ql3 in Discrete Neuronal Populations Controls Efferent Synapse Numbers and Diverse Behaviors. Neuron 91, 1034–1051. [PubMed: 27478018]

Matsuda K, Budisantoso T, Mitakidis N, Sugaya Y, Miura E, Kakegawa W, Yamasaki M, Konno K, Uchigashima M, Abe M, et al. (2016). Transsynaptic Modulation of Kainate Receptor Functions by C1q-like Proteins. Neuron 90, 752–767. [PubMed: 27133466]

Matsuda K, Miura E, Miyazaki T, Kakegawa W, Emi K, Narumi S, Fukazawa Y, Ito-Ishida A, Kondo T, Shigemoto R, et al. (2010). Cbln1 Is a Ligand for an Orphan Glutamate Receptor d2, a Bidirectional Synapse Organizer. Science 338, 1541–1545.

Matsutani S, and Yamamoto N (2008). Centrifugal innervation of the mammalian olfactory bulb. Anat. Sci. Int 83, 218–227. [PubMed: 19159349]

Nagayama S, Homma R, and Imamura F (2014). Neuronal organization of olfactory bulb circuits. Front. Neural Circuits 8, 1–19. [PubMed: 24478635]

Neville KR, and Haberly LB (2004). Olfactory cortex In The Synaptic Organization of the Brain, Shepherd GM, ed. (New York: Oxford University Press), pp. 415–454.

Padmanabhan K, Osakada F, Tarabrina A, Kizer E, Callaway EM, Gage FH, and Sejnowski TJ (2016). Diverse Representations of Olfactory Information in Centrifugal Feedback Projections. J. Neurosci 36, 7535–7545. [PubMed: 27413162]

Padmanabhan K, Osakada F, Tarabrina A, Kizer E, Callaway EM, Gage FH, and Sejnowski TJ (2019). Centrifugal inputs to the main olfactory bulb revealed through whole brain circuit-mapping. Front. Neuroanat 12, 1–11.

Pressler RT, and Strowbridge BW (2017). Direct Recording of Dendrodendritic Excitation in the Olfactory Bulb: Divergent Properties of Local and External Glutamatergic Inputs Govern Synaptic Integration in Granule Cells. J. Neurosci 37, 11774–11788. [PubMed: 29066560]

Price JL, and Powell TP (1970). An experimental study of the origin and the course of the centrifugal fibres to the olfactory bulb in the rat. J. Anat 107, 215–237. [PubMed: 5487119]

Ressl S, Vu BK, Vivona S, Martinelli DC, Südhof TC, and Brunger AT (2015). Structures of C1q-like proteins reveal unique features among the C1q/TNF superfamily. Structure 23, 688–699. [PubMed: 25752542]

Rochefort C, Gheusi G, Vincent JD, and Lledo PM (2002). Enriched odor exposure increases the number of newborn neurons in the adult olfactory bulb and improves odor memory. J. Neurosci 22, 2679–2689. [PubMed: 11923433]

Ross RS, and Eichenbaum H (2006). Dynamics of Hippocampal and Cortical Activation during Consolidation of a Nonspatial Memory. J. Neurosci 26, 4852–4859. [PubMed: 16672659]

Sacco T, and Sacchetti B (2011). Role of Secondary Sensory Cortices. Science 329, 649–657.

Shepherd GM, Chen WR, and Greer CA (2004). Olfactory bulb In The Synaptic Organization of the Brain, Shepherd GM, ed. (New York: Oxford University Press), pp. 165–216.

Sigoillot SM, Iyer K, Binda F, González-Calvo I, Talleur M, Vodjdani G, Isope P, and Selimi F (2015). The Secreted Protein C1QL1 and Its Receptor BAI3 Control the Synaptic Connectivity of Excitatory Inputs Converging on Cerebellar Purkinje Cells. Cell Rep. 10, 820–832. [PubMed: 25660030]

Stevens B, Allen NJ, Vazquez LE, Howell GR, Christopherson KS, Nouri N, Micheva KD, Mehalow AK, Huberman AD, Stafford B, et al. (2007). The Classical Complement Cascade Mediates CNS Synapse Elimination. Cell 131, 1164–1178. [PubMed: 18083105]

Südhof TC (2017). Synaptic Neurexin Complexes: A Molecular Code for the Logic of Neural Circuits. Cell 171, 745–769. [PubMed: 29100073]

Tang YT, Hu T, Arterburn M, Boyle B, Bright JM, Palencia S, Emtage PC, and Funk WD (2005). The complete complement of C1q-domain-containing proteins in Homo sapiens. Genomics 86, 100–111. [PubMed: 15953544]

Tervo DGR, Hwang B-Y, Viswanathan S, Gaj T, Lavzin M, Ritola K, Lindo S, Michael S, Kuleshova E, Ojala D, et al. (2016). A Designer AAV Variant Permits Efficient Retrograde Access to Projection Neurons. Neuron 92, 372–382. [PubMed: 27720486]

Uemura T, Lee SJ, Yasumura M, Takeuchi T, Yoshida T, Ra M, Taguchi R, Sakimura K, and Mishina M (2010). Trans-synaptic interaction of GluRδ2 and Neurexin through Cbln1 mediates synapse formation in the cerebellum. Cell 141, 1068–1079. [PubMed: 20537373]

Whitman MC, and Greer CA (2007). Synaptic integration of adult-generated olfactory bulb granule cells: basal axodendritic centrifugal input precedes apical dendrodendritic local circuits. J. Neurosci 27, 9951–9961. [PubMed: 17855609]

Wrenn CC (2004). Social transmission of food preference in mice: In Current Protocols in Neuroscience, pp. 8.5G.1–8.5G.7.

Xu W, and Südhof TC (2013). A neural circuit for memory specificity and generalization. Science 339, 1290–1295. [PubMed: 23493706]

Yamauchi T, Kamon J, Ito Y, Tsuhida A, Yokomizo T, Kita S, Sugiyama T, Miyagishi M, Hara K, Tsunoda M, et al. (2003). Cloning of adiponectin receptors that mediate antidiabetic metabolic. Nature 423, 762–769. [PubMed: 12802337]

Yan Z, Tan J, Qin C, Lu Y, Ding C, and Luo M (2008). Precise circuitry links bilaterally symmetric olfactory maps. Neuron 58, 613–624. [PubMed: 18498741]

Yuzaki M (2018). Two Classes of Secreted Synaptic Organizers in the Central Nervous System. Annu. Rev. Physiol 80, 243–262. [PubMed: 29166241]

Zipursky SL, and Sanes JR (2010). Chemoaffinity revisited: Dscams, protocadherins, and neural circuit assembly. Cell 143, 343–353. [PubMed: 21029858]

HIGHLIGHTS

- Anterior olfactory nucleus (AON) neurons express high levels of synaptogenic C1ql3
- AON deletion of C1ql3 blocks social transmission of food preference (STFP) learning
- Similarly, olfactory bulb deletion of the C1ql3 receptor Bai3 blocks STFP learning
- Presynaptic C1ql3 and postsynaptic Bai3 enable AON→olfactory bulb synapse function

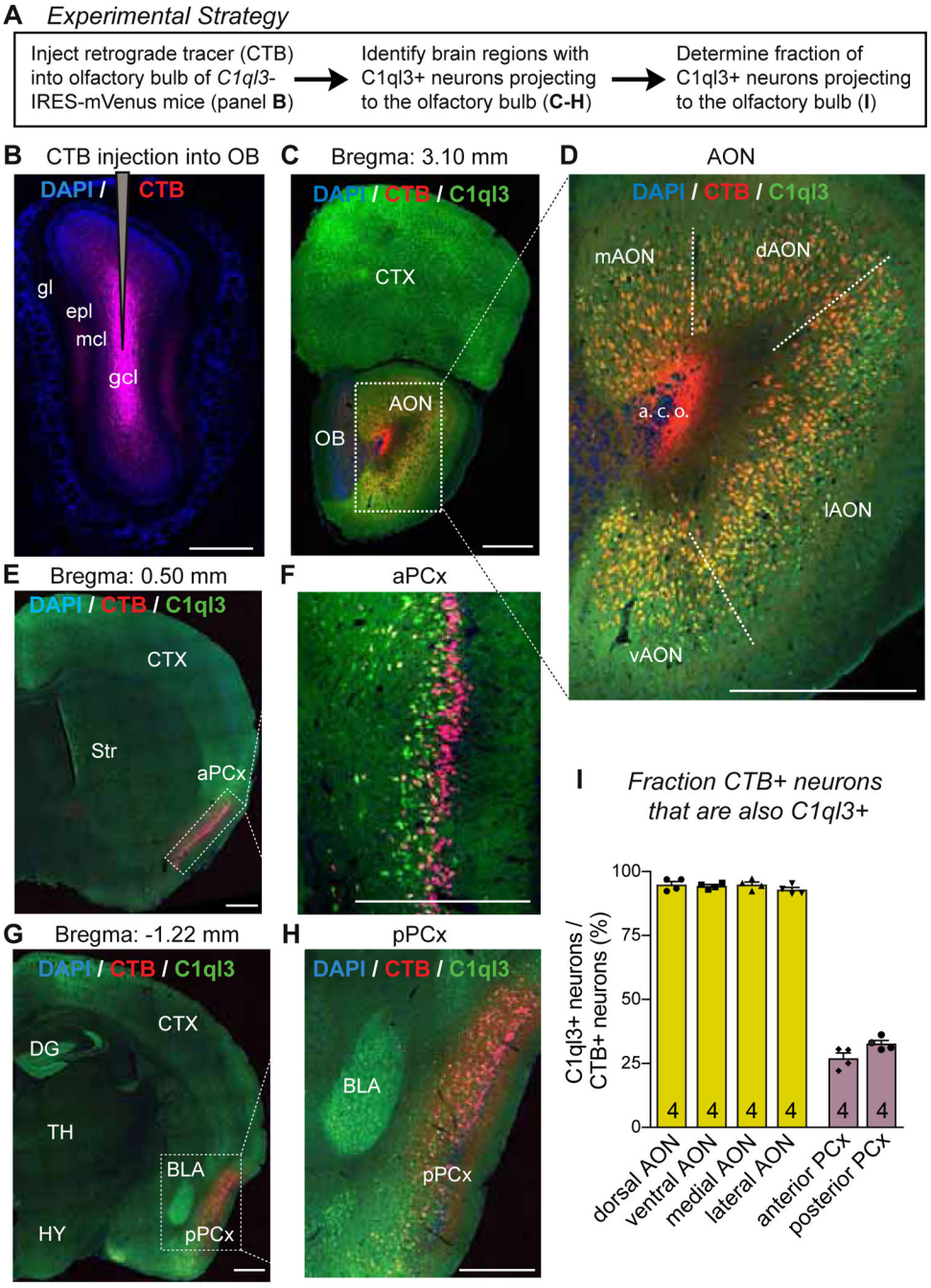

Figure 1. Nearly all neurons of the anterior olfactory nucleus (AON), but few neurons of the piriform cortex (aPCx), projecting to the olfactory bulb (OB) express C1ql3

(A) Experimental strategy.

(B) Representative image of the OB after CTB injection (gl: glomerular layer; epl: external plexiform layer; mcl: mitral cell layer; ipl: internal plexiform layer; gcl: granule cell layer). Scale bar = 500 μm.

(C-H) Representative images of C1ql3^{+} (green) and CTB^{+} neurons (red) in the anterior olfactory nucleus (AON; C & D), the anterior piriform cortex (aPCx; E & F), and the posterior piriform cortex (pPCx; G & H). (abbreviations: mAON, dAON, lAON and vAON,

pars medialis, dorsalis, lateralis, and ventralis of the AON; CTX, cortex; a.c.o., anterior commissure of the olfactory limb; Str, striatum; DG, dentate gyrus; TH, thalamus; HY, hypothalamus; BLA, basolateral amygdala). Scale bar = 500 μm.

(I) Summary graph of the percentage of $C1ql3^+$ neurons among CTB^+ neurons in different parts of the AON and the aPCx and pPCx that project to OB granule cells. Data are means ± SEM (n = 4 mice).

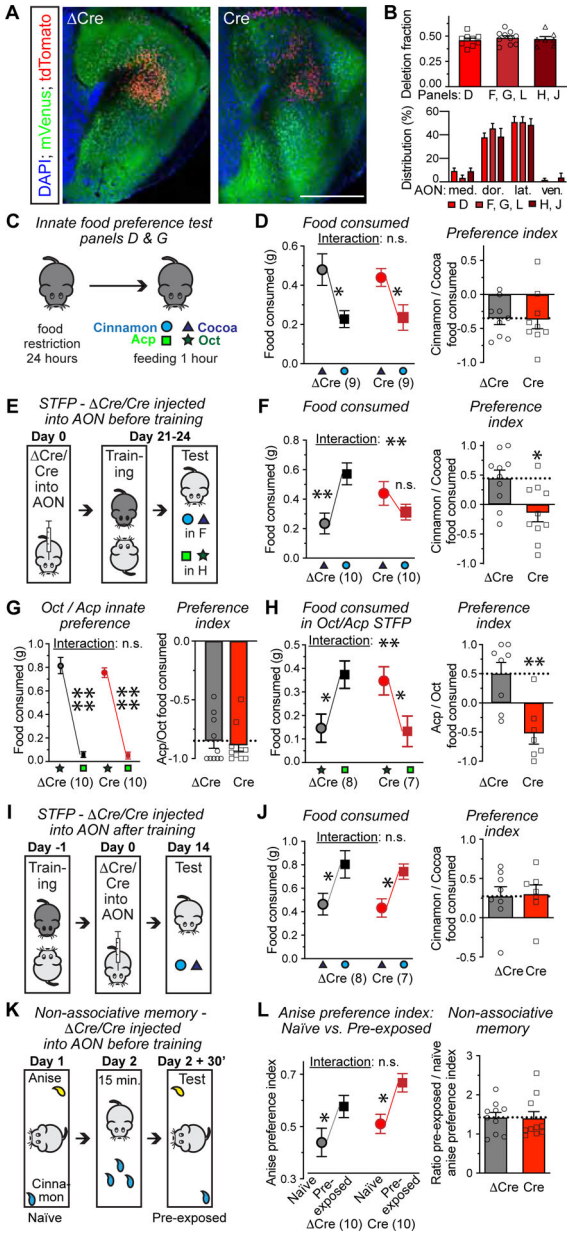

Figure 2. Conditional deletion of *C1ql3* in the AON abolishes memory acquisition during social transmission of food preference (STFP), but does not impair recall of STFP memory or a non-associative olfactory memory

(A) Representative images of the AON from *C1ql3 cKO* mice infected with AAVs expressing ΔCre- (left) or Cre-tdTomato (right). Cre ablates the mVenus signal (scale bar = 500 μm).

(B) The extent of the *C1ql3* deletion in the AON, measured as the fraction of AON neurons lacking mVenus (top), and the Cre-tdTomato distribution in the AON (bottom). Letters on the x-axis refer to the experimental panels below that used the same cohorts of mice.

(C & D) Innate food preference for cocoa vs. cinnamon (C, experimental paradigm; D, summary plot of consumed food (left), and cinnamon preference index [the difference

between consumed cinnamon and cocoa food divided by the total amount of food eaten] (right)).

(E) Strategy for testing the effect of an AON *C1ql3* deletion prior to STFP training on STFP memory. ΔCre- or Cre-expressing AAVs are injected into the AON of *C1ql3 cKO* observer mice on day 0. Food-restricted observer mice are exposed for 30 min to demonstrator mice that had just consumed food with cued odor (cinnamon or Acp) on day 21–24 (training), and observer mice are then given two food pellets with the cued and novel odor respectively (test).

(F) Summary of the amount of cinnamon- and cocoa-scented food consumed during STFP test (left) and the cinnamon preference index (right) for the experiment in E.

(G) Innate food preference for octanal (Oct) vs. acetophenone (Acp), similar paradigm as C.

(H) Summary of Oct vs. Acp STFP as a function of *C1ql3* deletion in the AON before training. (I-J) Strategy for testing the effect of deleting *C1ql3* in the AON after STFP training on STFP memory (I), and summary of the amount of cinnamon- and cocoa-scented food consumed during STFP test (left, J) and the cinnamon preference index (right, J).

(K) Strategy for testing the effect of deleting *C1ql3* in the AON on a non-associative olfactory memory. The time that mice sniffed 1% anise or 1% cinnamon odors is measured in a 10-min window (naïve). 24 h later, the same procedure is repeated 30 minutes after the mice were exposed to 1% cinnamon for 15 minutes in their home cage (pre-exposed).

(L) Summary of anise preference index (time investigating anise divided by that for cinnamon) in naïve vs. pre-exposed trials (left) and non-associative olfactory memory index measured by dividing the anise preference index in the pre-exposed trial by that of the naïve trial (right).

All data are means ± SEM (n = mouse numbers indicated in each panel; dots show individual data points). Statistical significance was assessed by *Student's* t-test in the right panels of D, FH, J and L, and by two-way ANOVA with Bonferroni's multiple comparison test in the left panels of D, F-H, J and L. No statistical significance was detected in the top panel of B using one-way ANOVA (*, $p<0.05$; **, $p<0.01$; 3*, $p<0.001$; 4*, $p<0.0001$).

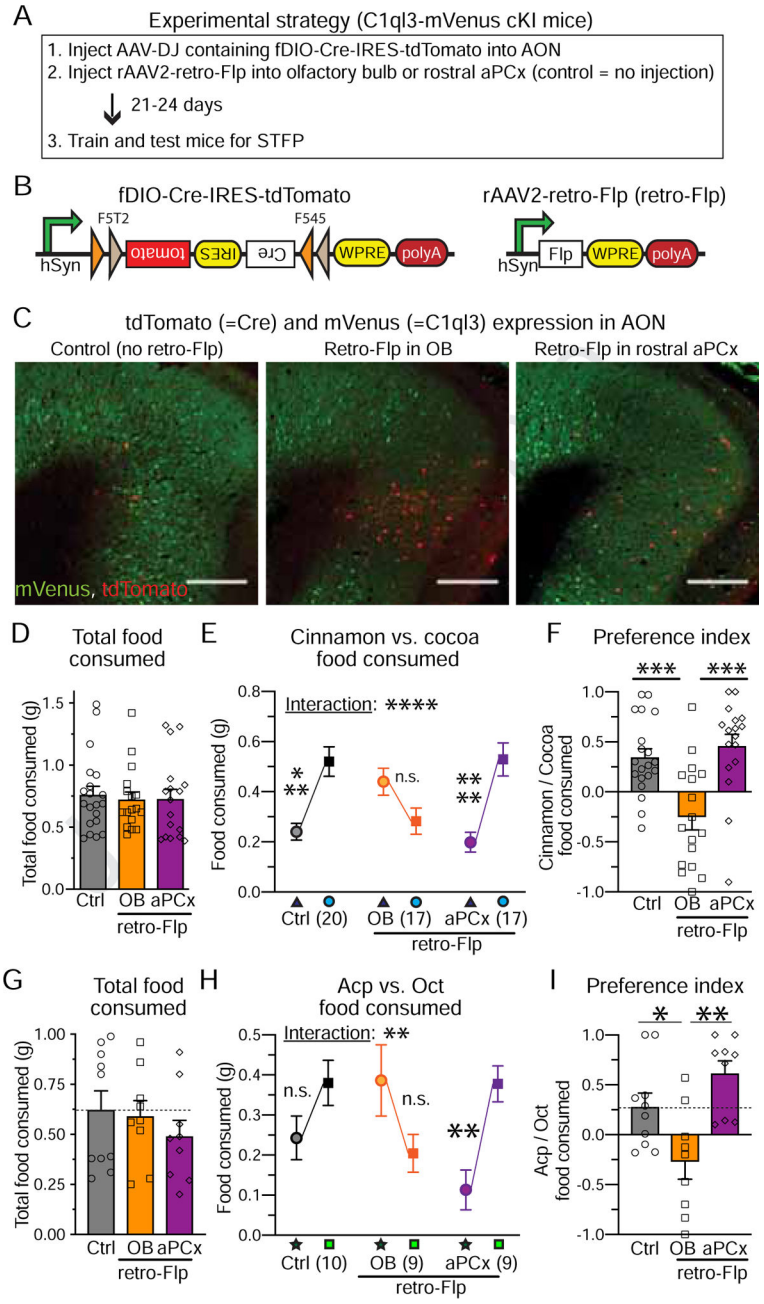

Figure 3. *C1ql3* in AON→OB- but not AON→piriform cortex-projecting neurons are essential for the acquisition of STFP memory

(A) Experimental strategy.

(B) Design of AAVs co-expressing Flp-dependent Cre together with tdTomato (left) and of rAAV2-retro expressing Flp (right).

(C) Representative images of the AON from all three groups. Scale bars = 500μm.

(D) Total food consumed during STFP tests.

(E) Amount of cocoa and cinnamon food consumed for all three groups during the STFP tests (triangle: cocoa; circle: cinnamon).

(F) Cinnamon preference index for all three groups in the STFP test.

(G-I) Same as D-F, but for the Acp vs. Oct odor pair (star: Oct; square: Acp).
All data are means ± SEM (n = mouse numbers indicated in each panel; dots show individual data points). Individual data points are indicated by dots. Statistical significance was assessed by one-way (D, F, G & I) or two-way ANOVA (E & H) with Bonferroni's multiple comparison test (*, $p<0.05$; **, $p<0.01$; 3*: $p<0.001$; 4*: $p<0.0001$).

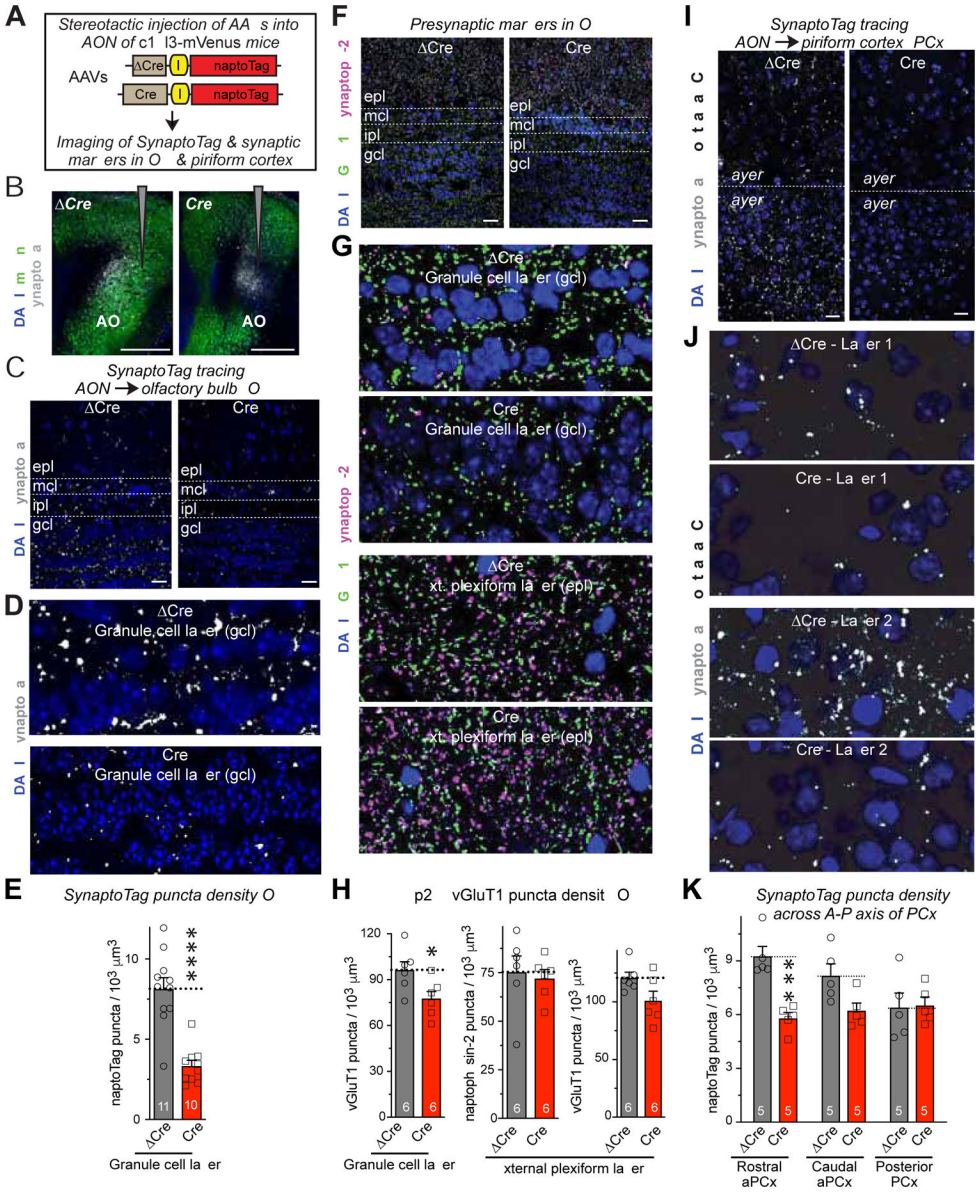

Figure 4. Deletion of *C1ql3* in the AON decreases the number of AON→OB granule cell synapses and of AON→piriform cortex synapses

(A) Experimental approach. SynaptoTag represents tdTomato-fused synaptobrevin-2 to label presynaptic terminals (Martinelli et al., 2016).

(B) Representative images of injection sites in the AON. Note that Cre but not ΔCre ablates the mVenus signal.

(C & D) Representative images of OB sections from *C1ql3 cKO* mice with ΔCre or Cre and SynaptotTag (gray) expression in the AON (C, overview of the OB; D, higher-resolution view of the granule cell layer (gcl) which are used for quantification).

(E) Summary graphs of the density of SynaptoTag-positive puncta in gcl as a function of the *C1ql3* deletion in the AON.

(F & G) Representative images of OB sections from *C1ql3 cKO* mice with ΔCre or Cre in the AON. Sections were labeled for the presynaptic markers vGluT1 (green) and

synaptophysin-2 (a.k.a. synaptoporin; magenta) and for DAPI (blue; F, overview of the OB; G, higher-resolution views of the granule cell layer (gcl, top two images) and external plexiform layer (epl, bottom two images). vGluT1 marks all excitatory synapses, whereas synaptophysin-2 marks inhibitory dendrodendritic synapses in the external plexiform layer. (H) Summary graphs of the density vGluT1-positive puncta in the gcl (left graph) and of synaptophysin-2- (middle graph) and vGluT1-positive puncta (right graph) in the OB epl as a function of the *C1ql3* deletion in the AON.

(I & J) Representative images of rostral anterior piriform cortex (PCx) sections from *C1ql3 cKO* mice with ΔCre or Cre and SynaptotTag (gray) expression in the AON (I, overview; J, higher-resolution view of layer 1 (top two images) and layer 2 (bottom two images)).

(K) Summary graphs of the density of SynaptoTag-positive puncta in the indicated parts of the piriform cortex, monitored as a function of the conditional KO of *C1ql3* in the AON (aPCx = anterior piriform cortex).

All data are means ± SEM (n = mouse numbers indicated in each panel; dots show individual data points). Statistical significance was assessed by *Student's* t-test in E and F, and by two-way ANOVA with Bonferroni's multiple comparison test in H (*, $p<0.05$; ***, $p<0.001$; ****, $p<0.0001$). All scale bars are 20 μm except in B, which is 500 μm.

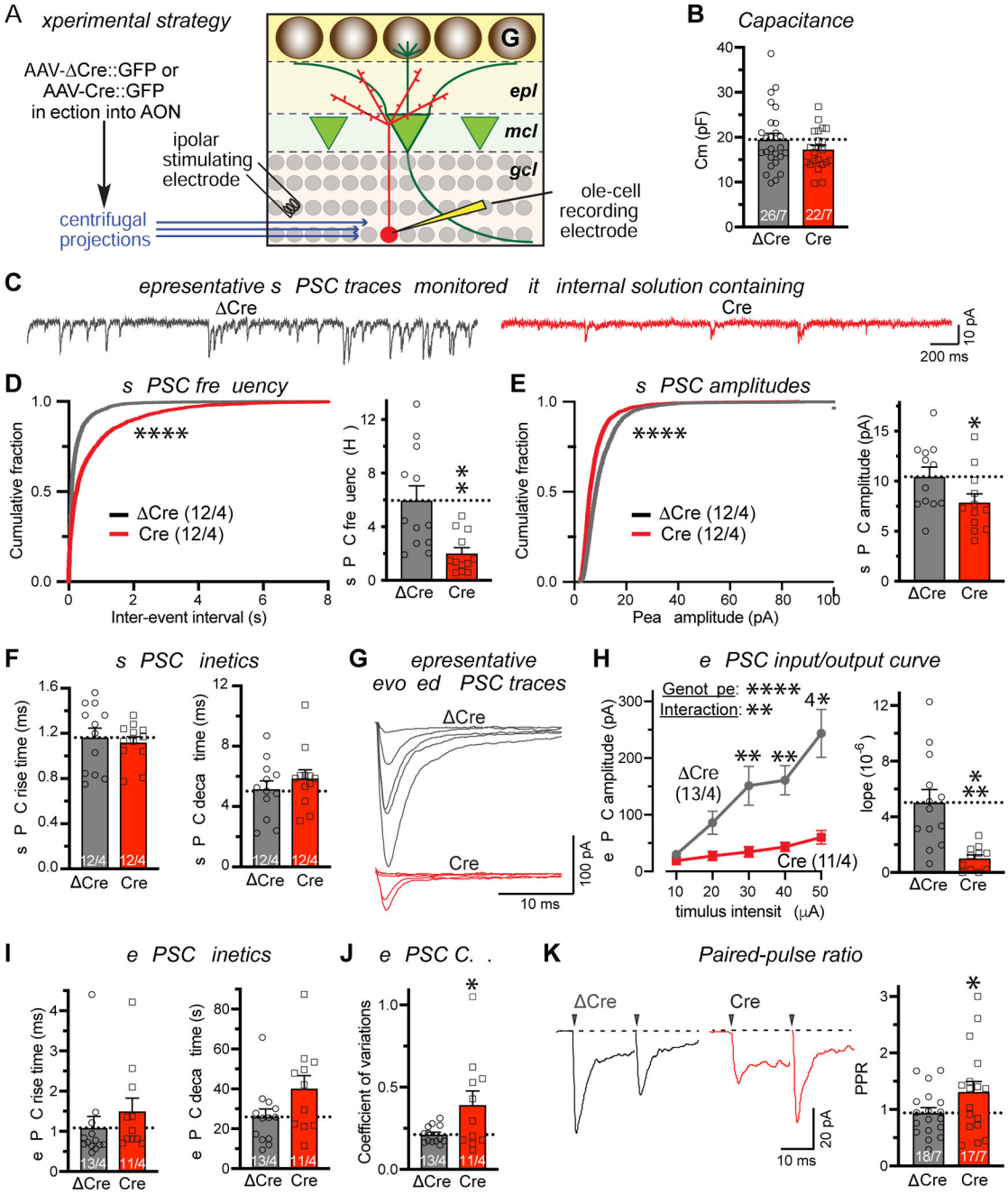

Figure 5. Deletion of C1ql3 in the AON suppresses centrifugal AON→OB granule cell synaptic transmission

(A) Experimental strategy. AAVs expressing EGFP-fused ΔCre or Cre were injected into the AON of P21–28 *C1ql3 cKO* mice. Whole-cell patch-clamp recordings were performed from granule cells in acute OB slices in the presence of picrotoxin (50 μM) in the bath and QX314 (10 mM) in the internal solution. Evoked EPSC were elicited by stimulating centrifugal projections with a bipolar concentric electrode in the granule cell layer near the recorded cell 30 μm below the surface.

(B) Summary of the granule cell capacitance as a function of *C1ql3* deletion in the AON.

(C-F) Summary of spontaneous EPSC (sEPSC) (C, representative traces; D, cumulative distribution of sEPSC inter-event intervals (left) and summary graph of the sEPSC frequency (right); E, cumulative distribution (left) and summary graph (right) of the sEPSC amplitude; F, sEPSC rise (10% to 90%) and decay times (90% to 10%)).
(G-I) Summary of evoked EPSCs (eEPSCs) at centrifugal synapses measured by input/output curve (G, representative traces; H, plot of the EPSC amplitude vs. stimulus strength (left) and slope of the EPSC amplitude vs. stimulus strength plots calculated for individual recordings (right); I, EPSC rise (10% to 90%) and decay (90% to 10%)).
(J & K) Summary of the indicators for the release probability at AON→OB granule cell synapses as measured by the coefficient of variation (J) and the paired-pulse ratio of eEPSCs (interstimulus interval, 20 ms) (K). Both measurements were with a 40 μA stimulus strength. All data are means ± SEM (n = cell numbers/mice indicated in each panel). Individual data points are indicated by dots. Statistical significance was assessed by Kolmogorov-Smirnov tests in the cumulative distributions of D and E, by *Student's* t-test in the summary graphs of D-K, and by two-way ANOVA with Bonferroni's multiple comparison test in the input/output curve in H (*, $p<0.05$; **, $p<0.01$; ***, $p<0.001$; ****, $p<0.0001$).

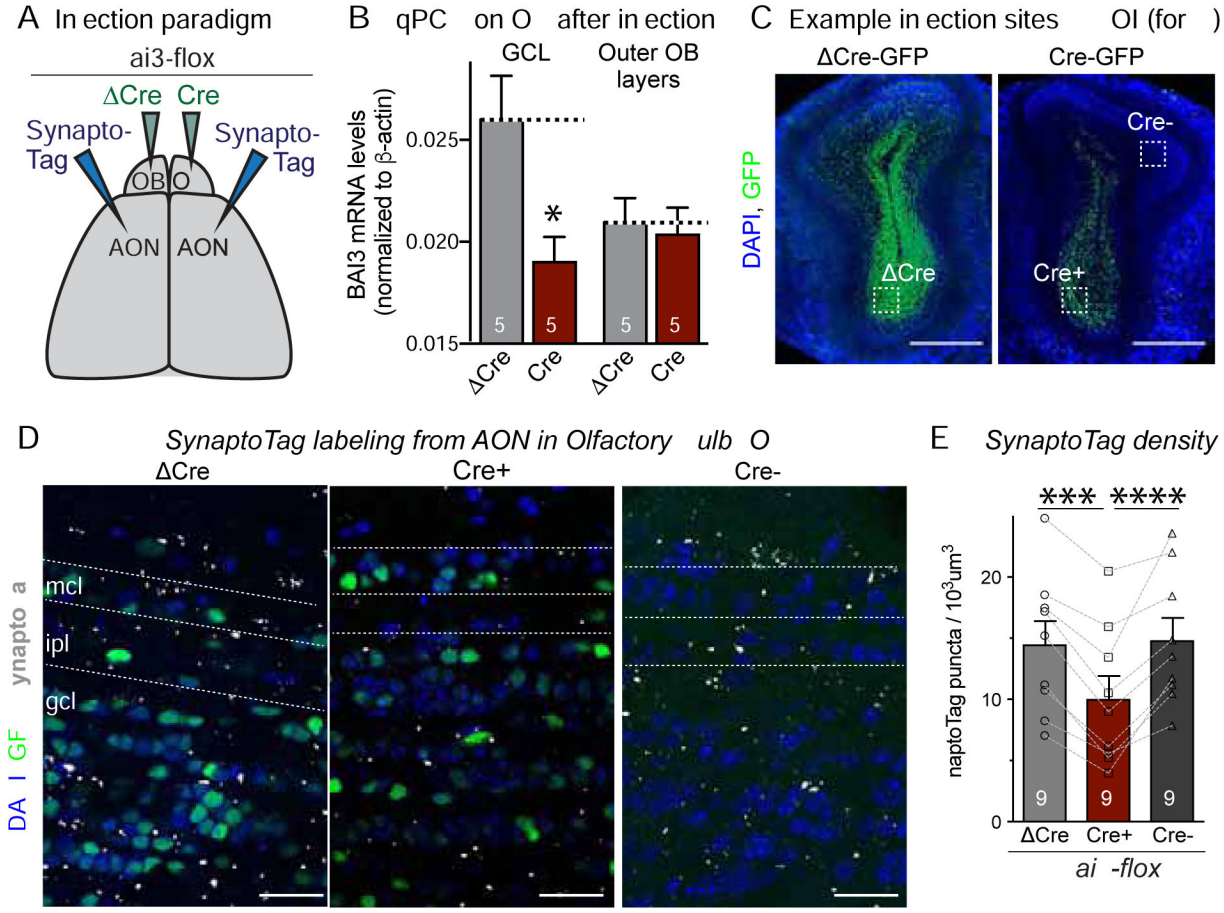

Figure 6. Postsynaptic deletion of the C1ql3 receptor Bai3 in OB granule cells decreases the density of AON→OB granule cell synapses

(A) Experimental strategy. AAVs expressing GFP-tagged ΔCre and Cre were randomly injected into one of the two olfactory bulbs of the same adult *Bai3 cKO* mouse, and AAVs expressing SynaptoTag were injected bilaterally into the AON. Three weeks later, SynaptoTag signals were quantified in the OB.

(B) RT-qPCR of Bai3 transcripts in different parts of the olfactory bulb. We dissected OB slices from mice obtained as described in A into an inner GCL part and an outer part. Bai3 mRNAs were measured in these samples and normalized to β-actin mRNA.

(C) Representative images of the olfactory bulb slices and regions of interests for analysis from the experiments described in A. GFP positive regions from ΔCre- or Cre-injected OBs from the same mice were analyzed as well as GFP negative regions from Cre-injected OBs as additional control (named Cre-). Scale bar = 500 μm.

(D) Representative images of the SynaptoTag signals in the OB. Scale bar = 20 μm.

(E) Summary of the SynaptoTag puncta density in the GCL analyzed in the EGFP-positive areas of ΔCre- or Cre-injected OBs as well as the EGFP-negative area of Cre-injected OBs from the same mouse.

All data are means ± SEM (n = mouse numbers indicated in each panel; dots indicate individual data points). Statistical significance was assessed by one-way paired (E) or two-

way ANOVA (B) with Bonferroni's multiple comparison test (*, $p<0.05$; **, $p<0.01$; ***, $p<0.001$; ****, $p<0.0001$).

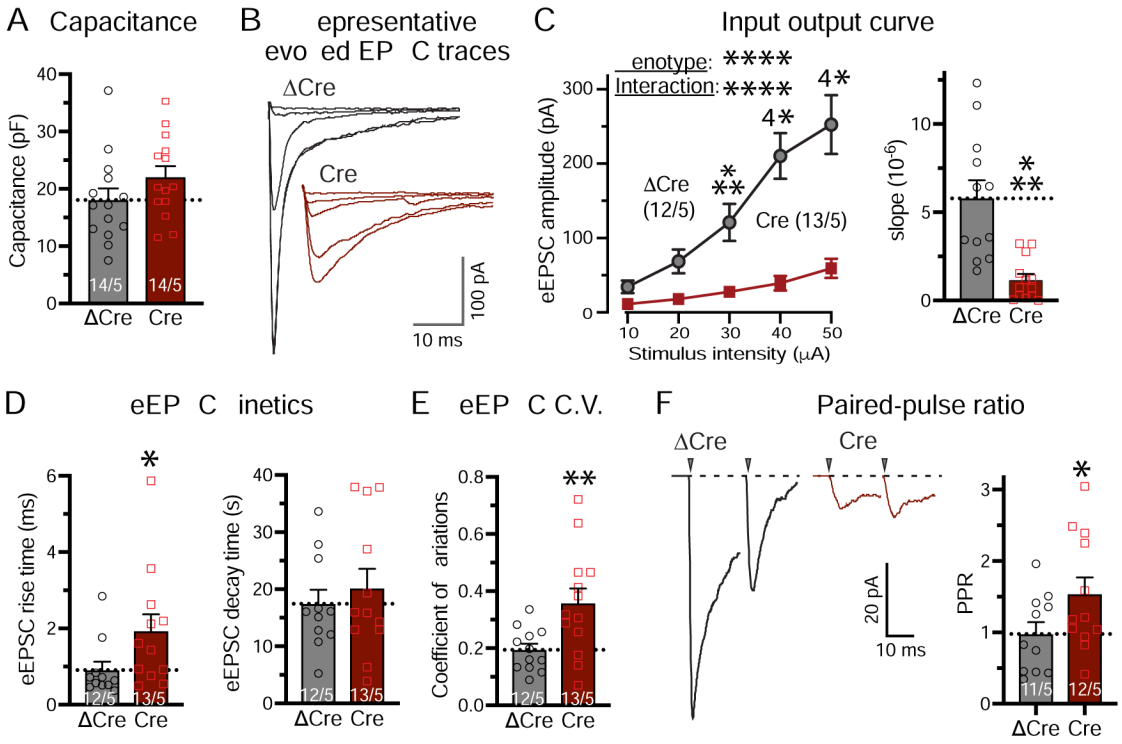

Figure 7. Postsynaptic deletion of *Bai3* in OB granule cells suppresses centrifugal synaptic transmission to granule cells in OB.

AAVs expressing EGFP-ΔCre or -Cre were injected into the OB of P21–28 *Bai3 cKO* mice, and whole-cell patch-clamp recordings were performed in EGFP-positive granule cells similar to Fig. 4.

(A) Summary of the granule cell capacitance as a function of *Bai3* deletion.

(B-D) Summary of evoked EPSCs (eEPSCs) at centrifugal synapses measured by input/output curve (B, representative traces; C, plot of the EPSC amplitude vs. stimulus strength (left) and slope of the EPSC amplitude vs. stimulus strength plots calculated for individual recordings (right); D, rise and decay times (10% to 90% and 90% to 10%, respectively)).

(E & F) Summary of the indicators for release probability at centrifugal synapses onto granule cells as measured by the coefficient of variation (E) and the paired-pulse ratio of eEPSCs (interstimulus interval, 20 ms)(F). Both measurements were with 40 μA stimulus strength.

All data are means ± SEM (n = number of cells/mice is indicated in each panel; dots show individual data points). Statistical significance was assessed by two-way ANOVA with Bonferroni's multiple comparison test in C, and by *Student's* t-test in the summary graphs of A-F (*, p<0.05; **, p<0.01; ***, p<0.001; ****, p<0.0001).

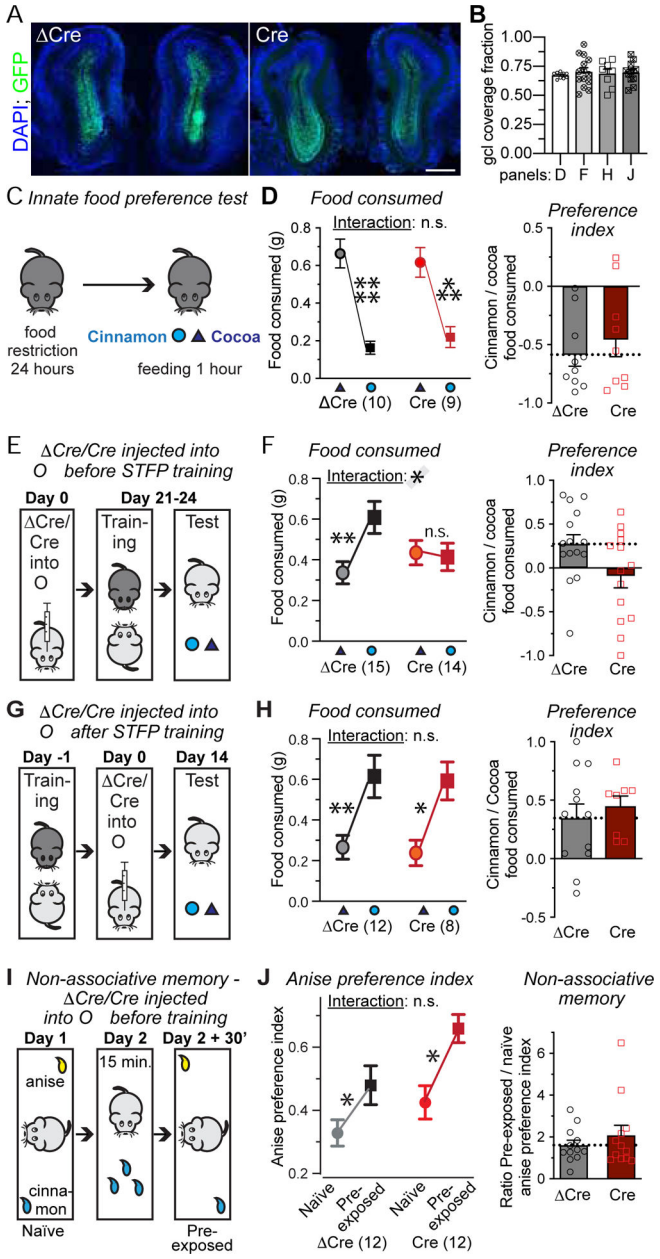

Figure 8. Deletion of *Bai3* in the OB blocks STFP memory acquisition without affecting STFP memory recall or non-associative olfactory memory.

(A) Representative images of EGFP-ΔCre or EGFP-Cre injected OBs (scale bars = 500 μm).

(B) The extent of the *Bai3* deletion in the OB, measured as the fraction of the GCL with Cre. Letters on the x-axis refer to the experimental panels below that used the same cohorts of mice.

(C & D) Innate food preference as a function of *Bai3* deletion in OB. (C, experimental paradigm; D, food consumed (left), and innate food preference index (right)).

(E & F) STFP memory as measured with cinnamon- and cocoa-scented food as a function of *Bai3* deletion in OB before training (E, experimental strategy; F, amount of cinnamon- and

cocoa-scented food consumed during STFP test (left), and cinnamon preference index (right).

(G & H) STFP memory as a function of *Bai3* deletion in OB after training (G, experimental strategy; H, amount of cinnamon- and cocoa-scented food consumed during STFP test (left), and cinnamon preference index (right)).

(I & J) Non-associative olfactory memory (I, experimental strategy [same as Figure 2K]; J, anise preference index in the 'naïve' and 'pre-exposed' trials (left), and non-associative olfactory memory index (right)).

All data are means ± SEM (n = mouse numbers indicated in each panel; dots show individual data points). Statistical significance was assessed by *Student's* t-test in the left panels of D, F, H & J, or two-way ANOVA with Bonferroni's multiple comparison test in the right panels of D, F, H & J (*, $p<0.05$; **, $p<0.01$; ***: $p<0.001$; ****: $p<0.0001$). No significance was detected in B by one-way ANOVA.

KEY RESOURCE TABLE

REAGENT or RESOURCE	Source	Identifier
Odor chemicals		
Ground cinnamon	McCormick	N/A
Cocoa powder	Hershey's	N/A
Acetophenone	Sigma-Aldrich	Cat # A10701
Octanal	Sigma-Aldrich	Cat # O5608
Cinnamon extract	Watkins	N/A
Anise extract	Watkins	N/A
Antibodies		
GFP	Invitrogen	Cat # A111–22; RRID: AB_221569
vGluT1	Millipore	Cat # AB5905; RRID: AB_2301751
Synaptophysin-2	Fykse et al., 1993	Y941
NeuN	Millipore	Cat # MAB377; RRID: AB_2298772
Virus strains		
AAV_{DJ}-ΔCre::GFP	Stanford Vector Core	N/A
AAV_{DJ}-Cre::GFP	Stanford Vector Core	N/A
AAV_{DJ}-ΔCre-IRES-tdTomato::Syb2	Stanford Vector Core	N/A
AAV_{DJ}-Cre-IRES-tdTomato::Syb2	Stanford Vector Core	N/A
AAV_{DJ}-mCherry-IRES-EGFP::Syb2	This manuscript	N/A
AAV_{DJ}-DIO-mCherry-IRES-EGFP::Syb2	This manuscript	N/A
AAV_{DJ}-fDIO-Cre-IRES-tdTomato	This manuscript	N/A
rAAV2-retro-Cre	This manuscript	N/A
rAAV2-retro-Flp	This manuscript	N/A
Chemicals		
Picrotoxin	Tocris	Cat # 1128
TTX	Fisher Scientific	Cat # 50-753-2807
QX314-Bromide	Tocris	Cat # 1014
Experimental Models: Organisms/Strains		
Mouse: C57BL/6J	The Jackson Lab	Jax Stock # 000664
Mouse: *C1ql3 cKO*	Martinelli et al., 2016	Deposited in the Jackson Lab; Jax Stock # 029672
Mouse: *Bai3 cKO*	Kakegawa et al., 2015	N/A
Mouse: *Nrxn3 cKO*	Aoto et al., 2015	N/A
Software		
Clampfit 10	Molecular Devices	https://www.moleculardevices.com/products/axon-patch-clamp-system/acquisition-and-analysis-software/pclamp-software-suite
NIS-Elements	Nikon	https://www.microscope.healthcare.nikon.com/products/software
Viewer III	Bioserve	http://www.biobserve.com/behavioralresearch/products/viewer/
Prism8	GraphPad	https://www.graphpad.com/scientific-software/prism/